Talanta 116 (2013) 809–815

Contents lists available at ScienceDirect

Talanta

journal homepage: www.elsevier.com/locate/talanta

Electrochemical immunoassay for carcinoembryonic antigen using gold nanoparticle–graphene composite modified glassy carbon electrode

Lian Zhu, Lili Xu, Ningming Jia, Baozhen Huang, Liang Tan*, Sufang Yang, Shouzhuo Yao

Key Laboratory of Chemical Biology and Traditional Chinese Medicine Research (Ministry of Education of China), College of Chemistry and Chemical Engineering, Hunan Normal University, Changsha 410081, PR China

ARTICLE INFO

Article history:
Received 5 June 2013
Received in revised form
20 July 2013
Accepted 27 July 2013
Available online 2 August 2013

Keywords:
Carcinoembryonic antigen
Immunoreaction
Electrochemical detection
Au nanoparticles
Graphene composites

ABSTRACT

Carcinoembryonic antigen (CEA), which is typically associated with certain tumors and developing fetus, is widely used as a clinical tumor marker for some familiar cancers. In this work, a simple and sensitive electrochemical CEA sensor was developed by employing immunoreaction. Gold nanoparticle–decorated graphene composites (Au–GN) were successfully synthesized based on the reduction of $HAuCl_4$ in the presence of graphene. Horseradish peroxidase-labeled anti-CEA antibody (HRP-anti-CEA) and HRP were successively adsorbed on the Au–GN modified glassy carbon electrode. The stepwise assembly process of the immunosensor was characterized by cyclic voltammetry and electrochemical impedance spectroscopy. The introduction of CEA antigens on the electrode surface reduced the electrochemical response of the electron transfer mediator due to the strong steric effect. Under the optimized conditions, the peak current change derived from the differential pulse voltammetry (DPV) measurements (ΔI_{DPV}) was proportional to the CEA concentration from 0.10 to 80 ng mL^{-1} with a detection limit of 0.04 ng mL^{-1} ($S/N=3$). In addition, this new protocol shows good selectivity, stability and reproducibility. The determination of CEA in human serum samples was performed and received in excellent accordance with the results determined by the enzyme-linked immunosorbent assay (ELISA).

1. Introduction

Immunoassays, a class of sensitive analytic approaches based on biospecific recognition interaction between antigen and antibody, have been widely employed in clinical diagnosis, environmental monitoring and food analysis [1–3]. Various immunoassay protocols, for example, radioassay, fluorescence, chemiluminescence, Raman spectroscopy, surface plasmon resonance and quartz crystal microbalance, have found their application in the determination of antigens or antibodies [4–9]. However, these methods are always suffering from radioactive contamination, time-consuming, qualified personnel and sophisticated instrumentation [10]. Compared with conventional immunoassay methods, electrochemical immunoassays have attracted considerable interest due to many advantages including high sensitivity, fast analysis, simple pretreatment, low cost and high compatibility with advanced micromachining technologies [11]. Electrochemical immunosensors have been developed for analysis of different biomarkers such as alpha-fetoprotein [12], human chorionic gonadotrophin [13] carbohydrate antigen 19-9 [14] and prostate specific antigen [15] based on amperometry, electrochemical impedance spectroscopy, potentiometry and conductometry.

Tumor markers are protein molecules that are associated with cancers and their detection can play an important role in early diagnosis and therapy of cancers [16]. Carcinoembryonic antigen (CEA), a kind of glycoprotein with molecular mass of about 200 kDa, is a reliable and widely used tumor maker. It is involved in cell adhesion and normally produced during fetal development but the production stops before birth [17]. The serum CEA level in an adult non-smoker is less than 2.5 ng mL^{-1} and for a smoker less than 5.0 ng mL^{-1}. High serum CEA level is related to some carcinomas such as lung cancer, ovarian carcinoma, breast cancer and colon cancer [18–21]. Thus, monitoring the level of CEA in human serum is necessary in clinical assay. In the last ten years, various amperometric immunoassays for CEA have been reported [22–30]. Developing a CEA immunosensor with good sensitivity and selectivity but without a complicated fabrication process still arouses researcher's considerable interest.

As we know, a crucial step for the construction of an electrochemical immunosensor is the immobilization of immunoreagent onto the electrode surface. Thus, searching for a suitable material for interface modification and an effective and simple immobilization

* Corresponding author. Tel./fax: +86 731 88872046.
E-mail address: liangtan@hunnu.edu.cn (L. Tan).

0039-9140/$ - see front matter © 2013 Elsevier B.V. All rights reserved.
http://dx.doi.org/10.1016/j.talanta.2013.07.069

method is of considerable interest in tests. Graphene (GN) is a novel class of 2D carbon-based nanomaterial in which sp^2 bonded carbon atoms are arranged into a honeycomb structure. It has attracted a great deal of interest due to its unique physical and chemical properties including high surface area, strong mechanical strength, excellent thermal conductivity and electric conductivity [31,32]. In recent years, one can find many reports on the graphene-based electrochemical sensors and biosensors owning excellent electric conductivity and electrocatalytic activity [33–40]. The extended long-range π-conjugation structure of graphene is beneficial to immobilization of some organic molecules with phenyl ring based on the π–π stacking interaction. The combination of graphene with different nanoscaled materials provides an electrochemical sensing platform with enhanced electronic and catalytic properties. Graphene-based composite materials have received increased attention due to synergistic contribution of two or more functional components and many potential applications [41]. Gold nanparticles (Au NPs) can exhibit quantum size effects with unique optical, electronic and catalytic properties. Au NPs are used increasingly in electrochemical bioassays since they can improve analytical sensitivity due to good conductivity and excellent compatibility with biomolecules [42,43]. The decoration of Au NPs to graphene creates a new nano-hybrid material with the integrated properties of the two components [44]. This nano-hybrid material can offer new opportunities for the development of biosensors with high analytical performance.

In the present work, gold nanoparticle–decorated graphene composites (Au–GN) were successfully synthesized based on the reduction of $HAuCl_4$ in the presence of graphene and this nano-hybrid material were characterized via transmission electron microscopy, UV–vis and infrared spectrophotometry. Horseradish peroxidase-labeled anti-CEA antibody was firstly immobilized on the Au–GN composite modified glassy carbon electrode surface. Next, horseradish peroxidase was used to block the nonspecific sites and to catalyze reduction of H_2O_2. The biospecific interaction between analyte, CEA antigens, and their antibodies assembled on electrode surface reduced the electrochemical response of the electron transfer mediator due to the strong steric effect. A sensitive CEA immunosensor with good selectivity, reproducibility and stability was developed.

2. Experimental

2.1. Materials and apparatus

CEA ELISA Kit was purchased from Autobio Diagnostic Co., Ltd. (China). Horseradish peroxidase (HRP) was obtained from Beijing Biosynthesis Biotechnology Co., Ltd. (China). Graphene was purchased from Nanjing CJNANO Tech Co., Ltd., (China). $HAuCl_4$ was obtained from Sinopharm Chemical Reagent Co., Ltd. (China). The buffer for the assay was 0.1 M phosphate buffered saline (PBS), prepared by mixing stock standard solution of Na_2HPO_4 and KH_2PO_4. Other chemicals including trisodium citrate, N, N-dimethylformamide (DMF), hydroquinone (HQ) and H_2O_2 were of analytical reagent grade and all aqueous solutions were prepared in Milli-Q ultrapure water. The breast cancer patients' serum samples were provided by the maternal and child health hospital of Hunan Province.

Electrochemical measurement experiments were performed with a CHI660C electrochemical workstation (CH Instruments, China) by using a three-electrode electrolytic cell. Glassy carbon electrode (GCE, 3 mm in diameter) acted as the working electrode. A KCl saturated calomel electrode served as the reference electrode. A platinum plate served as the counter electrode. The absorption spectra were recorded on a UV-2450 UV–vis spectrophotometer (Shimadzu, Japan). A Nicolet Nexus 670 FTIR spectrometer (Nicolet, USA) was employed for the infrared spectral measurements. The sizes of gold nanoparticle-decorated graphene composites were characterized ex situ by a Tecnai G^2 20ST transmission electron microscope (TEM, FEI, USA).

2.2. Preparation of gold nanoparticle–graphene composite (Au–GN) suspension

1.4 mg graphene was suspended in 2 mL ultrapure water by sonication for 30 min to make graphene dispersed equally. 200 μL 1% $HAuCl_4$ solution was added and the mixture solution was heated to boiling. Then 400 μL 0.1 M trisodium citrate was added to this solution drop by drop under vigorous stirring for 20 min. After the heating was stopped, the mixed solution was stirred continuously until it was cooled to room temperature. The prepared Au–GN composites were separated by centrifugation (13,000 rpm) and washed with ultrapure water for four times. Finally the precipitate was re-suspended with 2 mL DMF. It was stored in a brown glass bottle at room temperature.

2.3. Fabrication of immunosensor and measurement procedures

Prior to modification, GCE was polished with 0.05 μm α-Al_2O_3 power slurries until a mirror shiny surface appeared, and was sonicated sequentially in acetone, HNO_3 (1:1, v/v), NaOH (1 M) and double distilled water for 3 min. The treated electrode was scanned between −1.0 and 1.0 V versus SCE in 0.5 M H_2SO_4 aqueous solution for sufficient cycles to obtain reproducible cyclic voltammograms. A schematic drawing to illustrate the assembly process of immunosensor is shown in Fig. 1. After the electrode was thoroughly rinsed with doubly distilled water and dried with a stream of nitrogen gas, 3 μL of the prepared Au–GN suspension was dropped on the GCE surface and allowed to dry at room temperature. Subsequently, 5 μL of HRP labeled anti-CEA antibody (HRP-anti-CEA) solution was cast on the electrode surface and allowed to dry in refrigerator for overnight. Finally, 4 μL of 6 mg mL^{-1} HRP solution was employed to block the non-specific sites on the antibody-modified electrode. The prepared electrode was marked as HRP/HRP-anti-CEA/Au–GN/GCE and preserved in a refrigerator at 4 °C before use. The electrode was gently washed with PBS and then nitrogen-dried after every assembly process.

All electrochemical experiments were carried out at the ambient temperature of the laboratory (25 °C) in pH 7.5 PBS buffer as the supporting electrolyte. The electrochemical measurements of the bare GCE and modified GCEs were performed in 0.1 M pH 7.5 PBS containing 2 mM $K_3Fe(CN)_6$, 2 mM $K_2Fe(CN)_6$ and 0.1 M NaCl by cyclic voltammetry (CV) and electrochemical impedance spectroscopy (EIS). The frequency range was between 5 mHz and 100 kHz with signal amplitude of 5 mV. The differential pulse voltammetry (DPV) measurements for CEA detection were performed from 0.20 to −0.28 V with a pulse amplitude of 25 mV and width of 50 ms in nitrogen-saturated pH 7.5 PBS containing 8 mM HQ and 10 mM H_2O_2.

3. Results and discussion

3.1. Characterization of Au–GN composite

Fig. 2A shows the TEM image of Au–GN composite. It consists of an ultrathin transparent nanosheet decorated with individual and separated gold particles with the diameter of 50–100 nm. GN exhibits typical crumpled and wrinkled structure on the rough surface of the film and gold nanoparticles were uniformly anchored on the whole graphene sheets. Fig. 2B shows the UV–vis spectra of the GN, Au NPs and Au–GN composite in

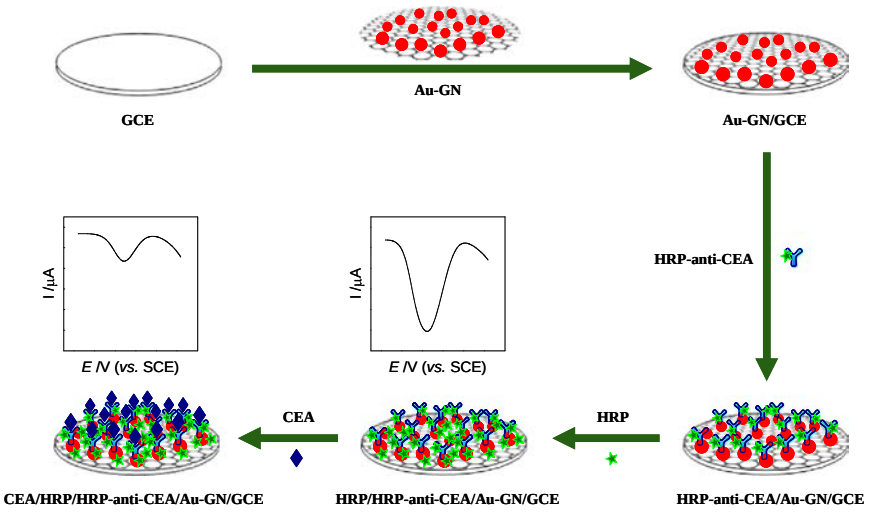

Fig. 1. Schematic illustration of the immunosensor assembly process.

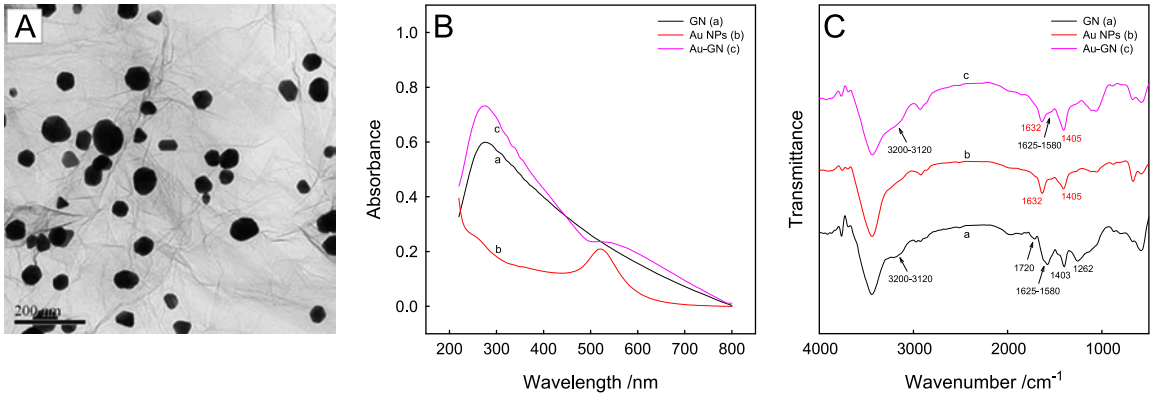

Fig. 2. TEM image of GNPs–GN composite (A). (B) UV–vis absorption spectra of aqueous dispersions containing GN (a), Au NPs (b) and Au–GN (c). (C) FTIR spectra of GN (a), Au NPs (b) and Au–GN (c).

aqueous solution from 240 to 800 nm, respectively. An obvious absorption peak in the spectrum of GN, which might be related to the ring-shaped conjugated structure of carbon atoms in graphene, could be found at 275 nm. Au NPs has prominent peaks at about 520 nm. The spectrum of Au–GN composite appeared to be an overlapping of two spectra for the GN and Au NPs but the absorption peak in the visible region is weakened and presents a plateau. FTIR spectra of GN, Au NPs and Au–GN composite in the range of 4000–500 cm^{-1} are shown in Fig. 2C. For GN, the weak and wide absorption band at 3200–3120 cm^{-1} may be due to the stretching vibration of C–H. The wide absorption band at 1625–1580 cm^{-1} was attributed to the stretching vibration of C=C in π-conjugation structure of graphene. The absorption bands at ~1720 and ~1262 cm^{-1} were derived from the C=O and C–O stretching vibration of carboxylic group (COOH), respectively. The absorption band at ~1403 cm^{-1} represented the in-plane OH deformation vibration of COOH. The above results suggest that some COOH groups were present at the graphene surface. The characteristic peaks of Au NPs at ~1632 and ~1405 cm^{-1} were ascribed to the stretching vibration of COO^-, which indicates that citrate was adsorbed on the Au NPs that were prepared based on the redox reaction using $HAuCl_4$ and trisodium citrate. The absorption bands at 3200–3120, 1625–1580, ~1632 and ~1405 cm^{-1} can be found in the spectrum of Au–GN. It is reported that the oxygen functional groups in graphene are responsible for a previous attachment of Au (III) ($HAuCl_4$) in solution owing to electrostatic interactions. Afterward, the addition of the reducing agent, such as citrate ion, to the precursor solution promotes the subsequent reduction of Au (III), enabling the growth of gold nanoparticles at the graphene surface [45]. The disappearance of the absorption bands at ~1720 and ~1262 cm^{-1} in the spectrum of Au–GN proved the transformation from COOH to COO–Au (III) at the graphene surface due to the electrostatic interactions. This change could promote the nucleation and growth of Au NPs based on the reduction of Au (III). The above TEM image, UV–vis and FTIR measurement results all indicate that Au NPs were strongly bound to graphene.

3.2. Electrochemical responses of the modified electrode

Cyclic voltammetry and electrochemical impedance spectroscopy is the powerful tools for investigating the interfacial properties of surface-modified electrode. The typical electrochemical interface can be represented as an electrical circuit including four parameters, the ohmic resistance of the electrolyte solution (R_s), the Warburg impedance (Z_w), the double-layer capacitance (C_{dl}) and the electron-transfer resistance (R_{et}). In general, a low frequency linear response and a high frequency semicircle in the Nyquist plot of impedance spectroscopy are characteristic of a mass-transfer controlled electrode process and a kinetic controlled process at the electrode interface, respectively [46]. R_s and Z_w represent bulk properties of the electrolyte solution and diffusion features of the redox probe in solution. C_{dl} and R_{et} reveal interfacial properties of the electrode, which is highly sensitive to the surface modification. R_{et} usually controls the interfacial electron-

transfer rate of the redox probe between the solution and the electrode and it equals the semicircle diameter at higher frequencies in the Nyquist plot of impedance spectroscopy. Fig. 3 shows cyclic voltammograms and electrochemical impedance spectra of modified glassy carbon electrodes before and after each step of modifications in pH 7.5 PBS using ferri-/ferrocyanide probe. The Au–GN composite-modified electrode presented bigger peak currents and smaller electron transfer resistance compared with bare glassy carbon electrode on which a couple of reversible redox peaks and a small semi-circle diameter of the Nyquist plot could be found. It indicates that the electric conductivity of the modified electrode was improved due to the Au–GN composites which owned large specific surface area as a good conductor. The introduction of HRP-anti-CEA resulted in a decrease of the peak currents and an increase of the electron transfer resistance, suggesting that the immobilization of the enzyme-labled antibodies on Au–GN composites was successfully achieved due to the S–Au bond and the π–π stacking interaction between proteins and nanocomposites. These proteins could efficiently block the electron transfer of electrochemical probe. The above two electrochemical parameters were changed to a greater extent with the addition of HRP, which proves that HRP could block the non-specific sites on the modified electrode. One can find the further decreased peak currents and increased Nyquist diameter after the capture of CEA antigens. It means that the electron transfer between solution and electrode was significantly inhibited by the immunoreaction of CEA with its antibody.

Fig. 4 shows the cyclic voltammograms of Au–GN/GCE, HRP-anti-CEA/Au–GN/GCE, HRP/HRP-anti-CEA/Au–GN/GCE and CEA/HRP/HRP-anti-CEA/Au–GN/GCE in nitrogen-saturated pH 7.5 PBS containing HQ and H_2O_2, respectively. A pair of redox peaks attributed to p-hydroquinone was presented on Au–GN/GCE. Both the anodic and cathodic peak current responses were decreased after the immobilization of HRP-anti-CEA, which suggests that the electron transfer between the electrode and the solution was weakened by the steric hindrance effect. The binding of HRP induced an increase of the cathodic peak current response and a decrease of the anodic peak current response. It is a typical electrocatalytic process. The following equations describe the reaction process.

$$\text{HRP (Red)} + H_2O_2 \rightarrow \text{HRP (Ox)} + H_2O \quad (1)$$

$$\text{HRP (Ox)} + \text{p-hydroquinone} \rightarrow \text{HRP (Red)} + \text{p-benzoquinone} \quad (2)$$

$$\text{p-benzoquinone} + e^- \rightarrow \text{p-hydroquinone (electrode reaction)} \quad (3)$$

HRP could catalyze the reduction of H_2O_2 and result in the oxidation of the electron medium, p-hydroquinone (Eqs. (1) and (2)). The oxidation product, p-benzoquinone, suffered electrochemical reduction on the electrode surface (Eq. (3)). When CEA antigens were added on to the electrode surface, they were bound with CEA antibodies and the Ab–Ag composites could further block the electron transfer due to the strong steric hindrance effect, leading to the diminished cathodic peak current response.

3.3. Condition optimization of electrochemical measurement

Some factors affecting the enzyme-catalyzed reactions were investigated, respectively. Fig. 5A and B shows the effect of the pH and the concentration of HRP immobilized on the modified electrode on the cathodic peak current change (ΔI_p), respectively. Here ΔI_p is the difference between the cathodic peak current response of HRP/HRP-anti-CEA/GNPs–GNs/GCE ($|I_{p,1}|$) and that of CEA/HRP/HRP-anti-CEA/GNPs–GNs/GCE ($|I_{p,2}|$), $|I_{p,1}| - |I_{p,2}|$, and $|I_{p,1}| > |I_{p,2}|$. One can find that the ΔI_p value was increased with the increase of the pH from 5.0 to 7.5, and then suffered a decrease

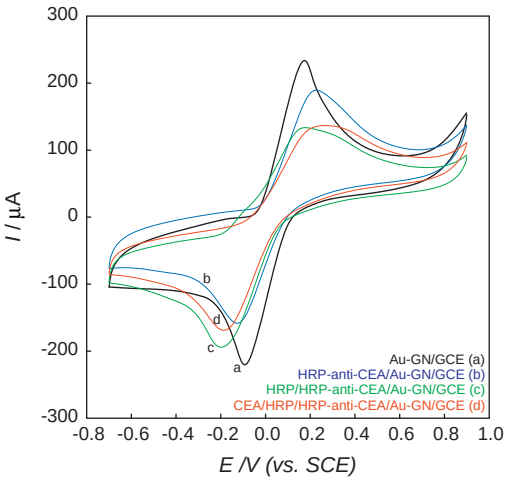

Fig. 4. Cyclic voltammograms of Au–GN/GCE (a), HRP-anti-CEA/Au–GN/GCE (b), HRP/HRP-anti-CEA/Au–GN/GCE (c) and CEA/HRP/HRP-anti-CEA/Au–GN/GCE (d) in nitrogen-saturated 0.1 M pH 7.5 PBS containing 10 mM H_2O_2 and 8 mM HQ. Sweep rate: 100 mV s^{-1}.

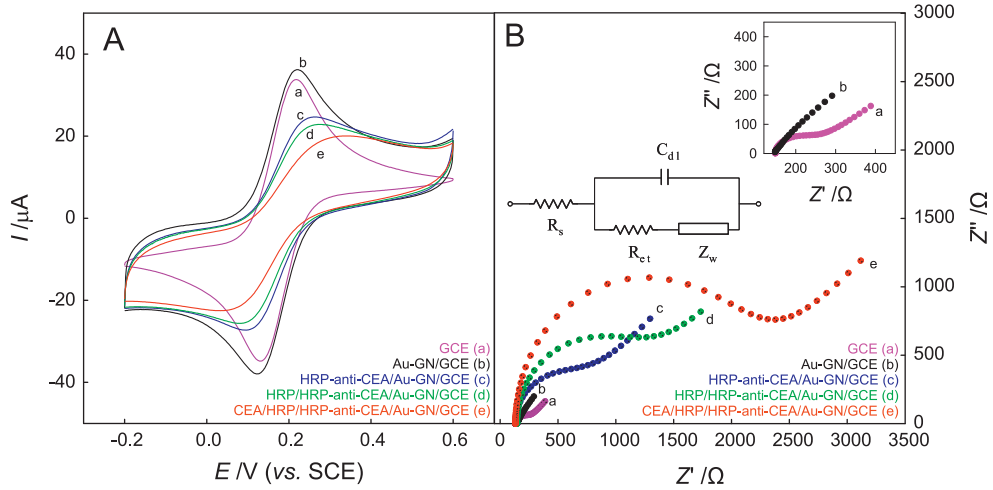

Fig. 3. Cyclic voltammograms (A) and electrochemical impedance spectra (B) of GCE (a), Au–GN/GCE (b), HRP-anti-CEA/Au–GN/GCE (c), HRP/HRP-anti-CEA/Au–GN/GCE (d) and CEA/HRP/HRP-anti-CEA/Au–GN/GCE (e) in 0.1 M pH 7.5 PBS containing 2 mM $K_3Fe(CN)_6$, 2 mM $K_2Fe(CN)_6$ and 0.1 M NaCl. Insert: the equivalent circuit and the magnified EIS of GCE (a) and Au–GN/GCE (b). (A) Scan rate: 50 mV s^{-1}; (B) AC frequency range: 100 kHz–5 mHz, amplitude: 5 mV, DC bias: 0.18 V vs. SCE.

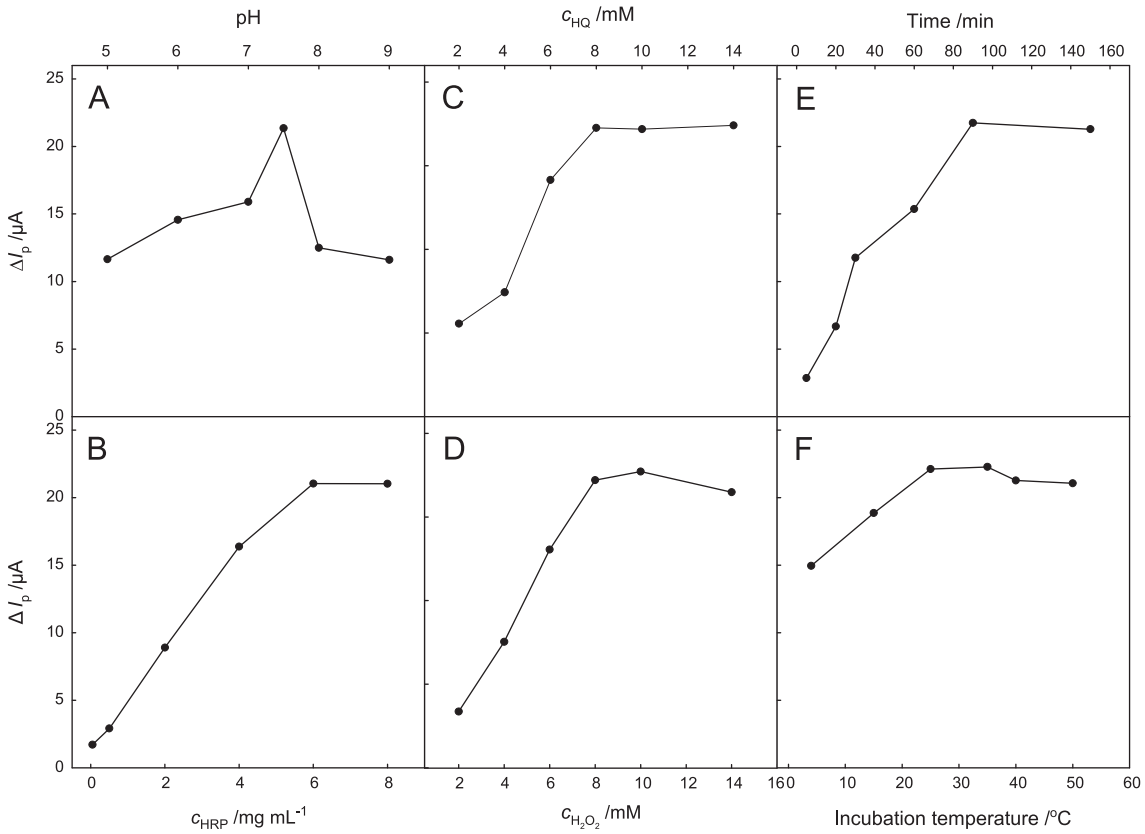

Fig. 5. Effects of the pH of solution (A), the concentration of HRP dropped on the modified electrode (B), the concentration of HQ (C), the concentration of H_2O_2 (D), the incubation time of CEA (E) and the incubation temperature of CEA (F) on the difference between the cathodic peak current response of HRP/HRP-anti-CEA/Au–GN/GCE and that of CEA/HRP/HRP-anti-CEA/Au–GN/GCE (ΔI_p).

when the pH was further enhanced from 7.5 to 9.0. It is known that most enzymes display good activity only in a limited range of pH [47]. As the maximum current response was achieved at pH 7.5, this pH was considered as the optimized pH for the proposed immunosensor. It is obvious that the ΔI_p value was increased with the enhancement of the HRP content and gradually reached a plateau when the c_{HRP} value exceeded 6 mg mL^{-1}. It indicates that the catalytic reactions were dominated by the amount of enzyme. Thus, the optimal concentration of HRP was selected at 6 mg mL^{-1}. The effect of the concentrations of HQ and H_2O_2 on the electrochemical measurements was also investigated and the results are shown in Fig. 5C and D, respectively. The performance of the electrochemical enzyme-catalyzed analysis was related to the concentration of HQ and H_2O_2 in the measuring system. The ΔI_p value in nitrogen-saturated 0.1 M pH 7.5 PBS was enhanced with the increasing concentrations of HQ and H_2O_2 from 2.0 to 8.0 mM and 2.0 to 10 mM, respectively, and then maintained the maximum value at higher concentrations. Therefore, the optimal HQ and H_2O_2 concentrations for the electrochemical enzyme-catalyzed analysis were 8.0 and 10 mM, respectively. As shown in Fig. 4, the added CEA antigens would be bound to their antibodies immobilized on the electrode surface, resulting in a decrease of the cathodic peak current response of the immunosensor. So it is imaginable that the reaction conditions of antigen and antibody could have effect on the electrochemical signal change. Fig. 5E and F indicates the effect of the incubation time and the incubation temperature of CEA on the cathodic peak current change, respectively. With an increasing incubation time the ΔI_p value was increased and tended to a maximum at 90 min. Longer incubation time did not enhance the electrochemical response change. When the incubation temperature ranged from 4 to 50 °C, the maximum ΔI_p value occurred at 35 °C. The lower response change at incubation temperatures higher than 35 °C should be attributed to the low activity of the enzyme due to the denaturation of bound enzyme during the incubation process. Hence the optimal conditions for CEA antigen assembly were chosen at 35 °C for 90 min.

3.4. Analytical performance of the immunosensor

The response of anti-CEA antibody modified electrode to CEA antigen reported in this work was employed for producing a CEA immunosensor. Fig. 6A shows the differential pulse voltammetry measurements using HRP/HRP-anti-CEA/GNPs–GNs/GCE in air-saturated pH 7.5 PBS containing CEA with increasing concentrations. The peak current decreased with positive shifts of peak potentials when the CEA content was enhanced. Fig. 6B exhibits plot of the peak current change (ΔI_{DPV}) before and after CEA introduction against the CEA concentration (c_{CEA}). Obviously the ΔI_{DPV} value rose with deflexibility when the c_{CEA} value was increased. It can be found from the insert of Fig. 5B that ΔI_{DPV} exhibited a linear response with respect to the logarithm of c_{CEA} ($\lg c_{CEA}$) over the range of CEA concentration from 0.10 to 80 ng mL^{-1}. The regression equations were $\Delta I_{DPV}=6.36\ \lg c_{CEA}+26.3$, with a high correlation coefficient of 0.982 and the detection limit for CEA was 0.04 ng mL^{-1}.

3.5. Specificity, stability and reproducibility of the developed immunosensor

As we know, specificity is an important factor of the immunosensor. To investigate the selectivity of the developed immunosensor, some proteins including 100 ng mL^{-1} α-1-fetoprotein (AFP), 100 U mL^{-1} ovarian cancer antigen 125 (CA-125) and 5 mg

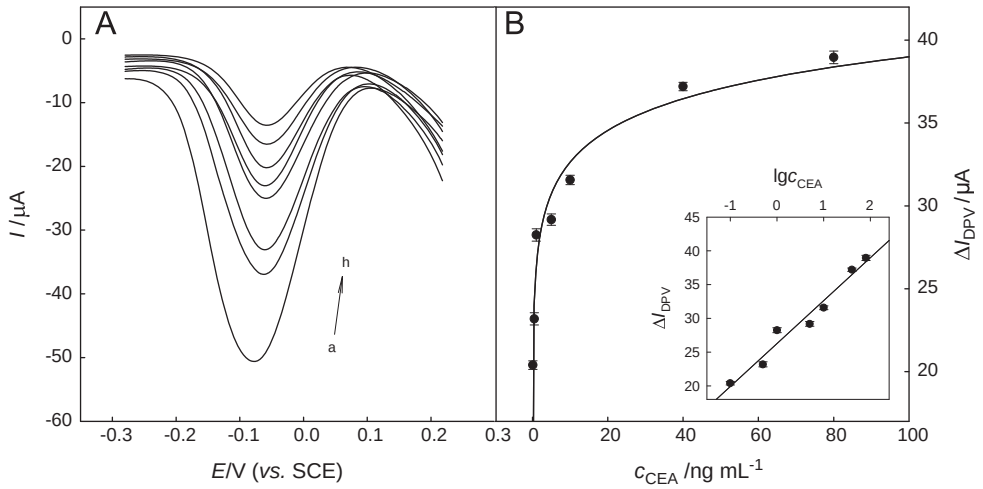

Fig. 6. (A) DPV responses of HRP/HRP-anti-CEA/Au–GN/GCE to CEA with different concentrations, from (a) to (h): 0, 0.1, 0.5, 1, 5, 10, 40, 80 ng mL^{-1}. Measuring solution: pH 7.5 PBS containing 8 mM HQ and 10 mM H_2O_2. (B) Plot of ΔI_{DPV} vs. c_{CEA}. Insert: Plot of ΔI_{DPV} vs lgc_{CEA}. Results are presented as mean ± SD (error bar) of triplicate experiments.

mL^{-1} BSA were used as the interference, respectively, to evaluate the specificity through comparing the electrochemical responses of 10 ng mL^{-1} of CEA antigen. As indicated from Fig. 7, a higher ΔI_{DPV} value was observed with the target CEA than those of other components. These results clearly demonstrated the high specificity of the electrochemical immunosensor. Two same HRP/HRP-anti-CEA/GNPs–GNs/GCEs were prepared, respectively. One was immediately used in the DPV measurements before and after the immobilization of 10 ng mL^{-1} CEA antigen. The other was stored at 4 °C for 10 days and then suffered the same test. It is found that the difference between the two ΔI_{DPV} values, which all were derived from the capture of CEA antigen, was lower than 5%. This experiment implies that the activity of anti-CEA antibody and HRP was effectively maintained and the immunosensor has a good stability. In order to study the reproducibility of the electrode preparation procedure, six modified electrodes based on the same fabrication procedure were prepared and used to investigate on the immobilization of 10 ng mL^{-1} CEA antigen. The RSD for the six ΔI_{DPV} values was calculated to be 3.4%, indicating that the developed immunosensor has a good reproducibility.

3.6. Evaluation of real samples

In order to investigate the analytical reliability of the proposed electrochemical method, the CEA concentrations in three clinical serum samples were detected using the present immunosensor and the assayed results were compared with those obtained by enzyme-linked immunosorbent assays (ELISA). As shown in Table 1, the absolute of the relative errors between the results derived from the two methods were from 2.3% to 4.1%. It suggests that the developed immunosensor provided a possible application for detection of CEA in clinical diagnostics.

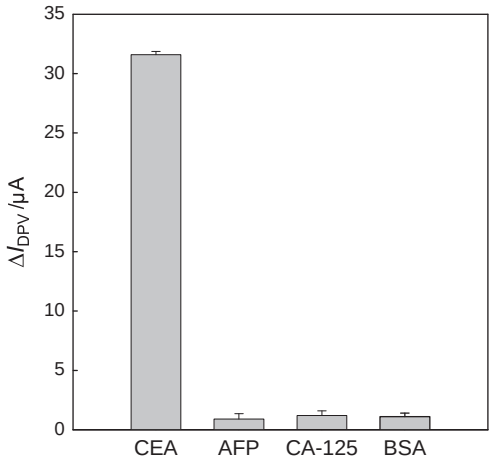

Fig. 7. The peak current change (ΔI_{DPV}) before and after addition of 10 ng mL^{-1} CEA, 100 ng mL^{-1} AFP, 100 U mL^{-1} CA-125 and 5 mg mL^{-1} BSA in DPV measurement using the proposed biosensor. Results are presented as mean ± SD (error bar) of triplicate experiments.

Table 1
Comparison of CEA determinations in human serum samples using two methods.

Serum number	Present immunosensor (ng mL^{-1})	ELISA (ng mL^{-1})	Relative error (%)
1	5.86	5.73	2.3
2	24.4	23.5	3.8
3	35.2	36.7	−4.1

4. Conclusions

In this study, Au–GN composites were fabricated using graphene based the reduction reaction of $HAuCl_4$ in solutions. HRP-anti-CEA was immobilized on the Au–GN modified electrode due to the Au-S bond and the π–π stacking interaction between biomolucules and the nanocomposites. HRP was cast on the modified electrode surface not only as a blocker for nonspecific sites but also as a catalyzer for redox reaction of HQ and H_2O_2. The immunoreaction between CEA antigens and HRP-anti-CEA provided the strong steric effect, which resulted in the notably decreased cathodic peak current response of HQ. The developed immunosensor showed an excellent performance for detection of CEA with a remarkable detection limit and acceptable selectivity, stability and reproducibility. Meanwhile, the electrochemical immunosensor was applied for the determination of clinical serum specimens, and the results were in accordance with those derived from ELISA. This sensitive electrochemical immunosensor shows promising potential for clinical applications.

Acknowledgments

This work was supported by the National Natural Science Foundation of China (20905025), Hunan Provincial Natural Science Foundation of China (12JJ3015), the Project of Hunan Provincial Science and Technology Program (2013NK3074), the Program for Excellent Talents in Hunan Normal University (ET12203) and Aid Program for Science and Technology Innovative Research Team in Higher Educational Institutions of Hunan Province.

References

[1] J.M.V. Emon, V. Lopez-Avila, Anal. Chem. 64 (1992) 78A–88A.
[2] A. Warsinke, A. Benkert, F.W. Scheller, J. Fresen, Anal. Chem. 366 (2000) 622–634.
[3] U. Bilitewski, Anal. Chem. 72 (2000) 692A–701A.
[4] B. Law, Immunoassay: A Practical Guide, Taylor & Francis, London, 1996.
[5] Z. Fan, Y.S. Keum, Q. Li, W.L. Shelver, L. Guo, J. Environ. Sci. 24 (2012) 1334–1340.
[6] C. Zong, J. Wu, J. Xu, H. Ju, F. Yan, Biosens. Bioelectron. 43 (2013) 372–378.
[7] J. Neng, M.H. Harpster, W.C. Wilson, P.A. Johnson, Biosens. Bioelectron. 15 (2013) 316–321.
[8] O.V. Gnedenko, Y.V. Mezentsev, A.A. Molnar, A.V. Lisitsa, A.S. Ivanov, A.I. Archakov, Anal. Chim. Acta 759 (2013) 105–109.
[9] A.B. Mattos, T.A. Freitas, V.L. Silva, R.F. Dutra, Sens. Actuators B 161 (2012) 439–446.
[10] K. Huang, D. Niu, W. Xie, W. Wang, Anal. Chim. Acta 659 (2010) 102–108.
[11] Z. Zhong, W. Wu, D. Wang, D. Wang, J. Shan, Y. Qing, Zhi Zhang, Biosens. Bioelectron. 25 (2010) 2379–2383.
[12] H. Yang, Z. Li, X. Wei, R. Huang, H. Qi, Q. Gao, C. Li, C. Zhang, Talanta 111 (2013) 62–68.
[13] M. Tao, X. Li, Z. Wu, M. Wang, M. Hua, Y. Yang, Clin. Chim. Acta 412 (2011) 550–555.
[14] B. Gu, C. Xu, C. Yang, S. Liu, M. Wang, Biosens. Bioelectron. 26 (2011) 2720–2723.
[15] H. Wang, Y. Zhang, H. Yu, D. Wu, H. Ma, H. Li, B. Du, Q. Wei, Anal. Biochem. 434 (2013) 123–127.
[16] D. Faraggi, A. Kramar, Urol. Oncol. 5 (2000) 211–213.
[17] M. Grunnet, J.B. Sorensen, Lung Cancer 76 (2012) 138–143.
[18] L. Hernández, A. Espasa, C. Fernández, A. Candela, C. Martín, S. Romero, Lung Cancer 36 (2002) 83–89.
[19] M.J.A. Engelen, H.W.A. de Bruijn, H. Hollema, K.A. ten Hoor, P.H.B. Willemse, J.G. Aalders, A.G.J. van der Zee, Gynecol. Oncol. 78 (2000) 16–20.
[20] B. Jezersek, J. Cervek, Z. Rudolf, S. Novaković, Cancer Lett. 110 (1996) 137–144.
[21] E. Eppler, H. Hörig, H.L. Kaufman, P. Groscurth, L. Filgueira, Eur. J. Cancer 38 (2002) 184–193.
[22] Z. Dai, F. Yan, H. Yu, X. Hu, H. Ju, J. Immunol. Methods 287 (2004) 13–20.
[23] D. Tang, J. Ren, Anal. Chem. 80 (2008) 8064–8070.
[24] Y. Zhuo, R. Yu, R. Yuan, Y. Chai, C. Hong, J. Electroanal. Chem. 628 (2009) 90–96.
[25] F. Kong, M. Xu, J. Xu, H. Chen, Talanta 85 (2011) 2620–2625.
[26] A. Sun, G. Chen, Q. Sheng, J. Zheng, Biochem. Eng. J. 57 (2011) 1–6.
[27] H. Chen, D. Tang, B. Zhang, B. Liu, Y. Cui, G. Chen, Talanta 91 (2012) 95–102.
[28] Y. Cai, H. Li, Y. Li, Y. Zhao, H. Ma, B. Zhu, C. Xu, Q. Wei, D. Wu, B. Du, Biosens. Bioelectron. 36 (2012) 6–11.
[29] Q. Zhu, Y. Chai, R. Yuan, Y. Zhuo, J. Han, Y. Li, N. Liao, Biosens. Bioelectron. 43 (2013) 440–445.
[30] G. Sun, J. Lu, S. Ge, X. Song, J. Yu, M. Yan, J. Huang, Anal. Chim. Acta 775 (2013) 85–92.
[31] A.K. Geim, K.S. Novoselov, Nat. Mater. 6 (2007) 183–191.
[32] C. Lee, X. Wei, J.W. Kysar, J. Hone, Science 321 (2008) 385–388.
[33] J. Meyer, Science 5929 (2009) 875–877.
[34] J. Li, S. Guo, Y. Zhai, E. Wang, Anal. Chim. Acta 2 (2009) 196–201.
[35] S. Hou, M.L. Kasner, S. Su, K. Patel, R. Cuellari, J. Phys. Chem. C 35 (2010) 14915–14921.
[36] G. Zeng, Y. Xing, J. Gao, Z. Wang, X. Zhang, Langmuir 18 (2010) 15022–15026.
[37] E. Dubuisson, Z. Yang, K.P. Loh, Anal. Chem. 7 (2011) 2452–2460.
[38] D. Du, L. Wang, Y. Shao, J. Wang, M.H. Engelhard, Y. Lin, Anal. Chem. 3 (2011) 746–752.
[39] B. Unnikrishnan, S. Palanisamy, S. Chen, Biosens. Bioelectron. 39 (2013) 70–75.
[40] Y. Lai, J. Bai, X. Shi, Y. Zeng, Y. Xian, J. Hou, L. Jin, Talanta 107 (2013) 176–182.
[41] X. Liu, J. Mao, P. Liu, X. Wei, Carbon 2 (2011) 477–483.
[42] R.N. Goyal, V.K. Gupta, M. Oyama, N. Bachheti, Electrochem. Commun. 8 (2006) 65–70.
[43] L. Zhu, L. Xu, L. Tan, H. Tan, S. Yang, S. Yao, Talanta 106 (2013) 192–199.
[44] S. Pruneanu, F. Pogacean, A.R. Biris, S. Ardelean, V. Canpean, G. Blanita, E. Dervishi, A.S. Biris, J. Phys. Chem. C 47 (2011) 23387–23394.
[45] G. Goncalves, P.A.A.P. Marques, C.M. Granadeiro, H.I.S. Nogueira, M.K. Singh, J. Grácio, Chem. Mater. 21 (2009) 4796–4802.
[46] A.J. Bard, L.R. Faulkner, Electrochemical Methods: Fundamentals and Applications, 2nd edition, John Wiley & Sons, Inc, New York, 2001.
[47] J. Wang, W. Huang, Y. Liu, J. Cheng, J. Yang, Anal. Chem. 18 (2004) 5393–5398.